Research Article

Synchronization method for long-term evolution-based machine-type communication in low-power cellular Internet of Things

Rothna Pec[1], Joo-Hyung Choi[1], Chang-Hwan Park[2] and Yong Soo Cho[1]

Abstract

The significant growth of machine-to-machine applications for low-power cellular Internet of Things has compelled 3rd Generation Partnership Project to ensure that the future release of long-term evolution can support massive transfer of small, infrequent packets using ultra-low-power and low-cost devices. The 3rd Generation Partnership Project version of machine-to-machine, called "machine-type communication," is currently being standardized for low-cost machine-type communication operations. In this article, a complete synchronization and cell search procedure is described for machine-type communication devices in long-term evolution systems. Low-complexity algorithms for primary synchronization signal and secondary synchronization signal detection, which requires the highest computational complexity in synchronization and cell search period, are also proposed for low-power machine-type communication devices. Through simulation under long-term evolution-based machine-type communication environments, we show that the proposed methods for primary synchronization signal and secondary synchronization signal detection require six and five times less computational complexity than the conventional methods, respectively, while their performance is similar. The proposed algorithms allow machine-type communication devices in a discontinuous reception cycle to resynchronize quickly with less power when synchronization is lost during a deep sleep period.

Introduction

The growing pervasiveness and ubiquity of small and cheap computing devices is paving the way for the realization of the Internet of Things (IoT) vision.[1,2] Several billions of such devices that use machine-to-machine (M2M) communication are predicted to come into existence over the next few years, and the majority of them are expected to be wireless sensors.[2–4] A large variety of communication technologies that connect such devices have emerged to support a large diversity of applications: Bluetooth in personal area networks, Zigbee in home automation systems, WiFi in local area networks, and cellular networks.[5–7]

[1]School of Electrical and Electronics Engineering, Chung-Ang University, Seoul, Republic of Korea
[2]Advanced Communication Technology Lab, LG Electronics, Seoul, Republic of Korea

Corresponding author:
Yong Soo Cho, School of Electrical and Electronics Engineering, Chung-Ang University, Seoul 06974, Republic of Korea.
Email: yscho@cau.ac.kr

The significant growth of M2M applications, such as smart metering, remote security sensing, energy management system, and healthcare monitoring, has compelled 3rd Generation Partnership Project (3GPP) and the cellular industry to ensure that the design and development of future long-term evolution (LTE) releases can support massive transfer of small, infrequent packets using very low-cost, low-complexity, and low-power devices.[8–10] The 3GPP version of M2M, called "machine-type communication" (MTC), was standardized in release 12 (Rel-12).[11] In Rel-12, a new profile, referred to as "category 0" (CAT-0) was defined for low-cost MTC operation. This evolved to a future release (Rel-13) that is currently being developed and is expected to be released in 2016.[4,12] The main objectives are to enhance the monitoring of service quality and support ultra-low-power, low-cost, and narrow-band user equipment (UE).[13,14] Eight of the world's leading standards bodies, including the European Telecommunications Standards Institute (ETSI) and Association of Radio Industries and Businesses (ARIB), have come together to create one M2M.[15,16]

Low-power consumption is a key requirement for enabling long battery life for MTC devices.[17,18] For example, some sensors/actuators installed inside the concrete could require a long time for battery replacement. Years of battery life might be required because replacing the battery is not an easy task. The low-power design is also required for cost reduction of MTC devices.[14] Discontinuous reception (DRX) mechanisms that allow receivers to turn their radio chip off during a predefined period have also been introduced for power saving.[19] DRX parameters, such as cycle period, sleeping time, and wake-up time, are controlled by networks, that is, eNodeB in LTE systems. A long sleep duration (up to several minutes) is allowed for MTC device (CAT-0).[20,21] However, the receiver might lose its synchronization while switching off its radio circuit. The MTC receiver needs to wake up earlier than the predefined time in order to perform synchronization before decoding any data in the control channels.[14,22] Therefore, a low-complexity synchronization method is required for MTC devices to shorten the period, thereby increasing sleeping duration (battery life). Furthermore, the MTC devices are allowed to use only one receive antenna at the minimum bandwidth for power-saving purposes.[6] Therefore, receive diversity gain cannot be obtained in MTC devices because they have only one antenna. However, MTC receivers can still obtain transmit diversity and repetition gains with their single antenna.[23]

In this article, we propose low-complexity synchronization methods that can reduce the power consumption of MTC devices during the synchronization period. The synchronization methods are developed based on two synchronization signals (primary synchronization signal (PSS) and secondary synchronization signal (SSS)) that have been used in legacy LTE systems.[24,25] A new synchronization signal cannot be designed for MTC devices, because the synchronization signals need to be compatible with legacy LTE systems. In order to complete downlink cell search, MTC devices also need to decode both master information block (MIB) and system information block (SIB) as UEs in legacy LTE systems. If cell ID is wrongly detected, decoding broadcast information is useless. Therefore, accurate synchronization with low-complexity algorithms using PSS and SSS is important for MTC devices. In this article, we describe a complete synchronization and cell search procedure for MTC devices. Two synchronization methods that can significantly reduce the computational complexity of MTC devices are proposed for PSS and SSS detection. The performance of the proposed methods is compared with those of conventional methods by simulation in LTE-based MTC environments.

The rest of this article is organized as follows. Section "Preliminaries" summarizes important characteristics of synchronization signals and physical channels required for the development of a synchronization and cell search algorithm in MTC devices. In section "Low-complexity synchronization methods for MTC devices," a complete synchronization and cell search procedure is described for MTC devices. Two low-complexity synchronization methods for PSS and SSS detection are also proposed for MTC devices. The simulation results are given in section "Simulation." Finally, a conclusion is drawn in the last section.

Preliminaries

In this section, we summarize important characteristics of synchronization signals and physical channels because MTC devices need to perform synchronization and cell searching using the synchronization signals and physical channels used in LTE systems. In the LTE system, two synchronization signals (PSS and SSS) are transmitted at the minimum bandwidth of 1.4 MHz in order to assist in the acquisition of synchronization parameters, such as symbol timing, carrier frequency offset (CFO), cyclic prefix (CP) type, frame timing, and cell ID. In addition, broadcast information is transmitted on two physical channels in order to assist in the completion of cell search. An MIB that carries information on the system bandwidth, system frame number, and physical channel hybrid ARQ indicator channel (PHICH) configuration is transmitted on the physical broadcast channel (PBCH). Another SIB that carries information such as public land mobile network (PLMN) ID and selection criteria is transmitted on the physical downlink share channel (PDSCH). A total of

504 unique physical cell identities (IDs) constructed by combining the cell ID group and cell ID within the cell ID group are supported

$$N_{ID}^{Cell} = 3N_{ID}^{(1)} + N_{ID}^{(2)} \qquad (1)$$

Here, $N_{ID}^{(1)} \in \{0, 1, \ldots, 167\}$ and $N_{ID}^{(2)} \in \{0, 1, 2\}$ denote the cell ID group and cell ID within the cell ID group, respectively.

PSS is generated in the frequency domain from 63-length Zadoff-Chu sequence (ZCS) with zero punctuation at the DC subcarrier component.[24,26] ZCS has good properties for synchronization signals, such as constant amplitude after fast Fourier transform (FFT) operation, ideal cyclic autocorrelation, and small cross-correlation value for any two ZCS whose root indices are relative prime. Three PSS with the root indices of 25, 29, and 34 are chosen to carry the information of cell IDs within the cell ID group. Each PSS is mapped to the 62 subcarriers around the DC component, thus occupying a system bandwidth of 1.08 MHz and allowing the use of the 64-FFT operation at the receiver. PSS is transmitted at the last orthogonal frequency-division multiplexing (OFDM) symbol of the first slot of subframes 0 and 5 for the frequency-division duplexing (FDD) mode, and at the third OFDM symbol of subframes 1 and 6 for the time-division duplex (TDD) mode. PSS is defined as follows

$$\tilde{X}_{PSS}^{u}(i) = \begin{cases} e^{-j\frac{\pi u i(i+1)}{63}}, & i = 0, 1, \ldots, 30 \\ e^{-j\frac{\pi u(i+1)(i+2)}{63}}, & i = 31, 32, \ldots, 61 \end{cases} \qquad (2)$$

where $u \in \{25, 29, 34\}$ denotes the root indices mapped to $N_{ID}^{(2)} \in \{0, 1, 2\}$. PSS is mapped in the frequency domain as follows

$$X_{PSS}^{u}(k) = \begin{cases} \tilde{X}_{PSS}^{u}(k + 31), & -31 \leq k < 0 \\ \tilde{X}_{PSS}^{u}(k + 30), & 0 < k \leq 31 \\ 0, & \text{otherwise} \end{cases} \qquad (3)$$

In equation (3), k denotes the subcarrier index that runs from $-N/2$ to $N/(2-1)$. Here, N denotes the FFT size. The time-domain signal, $x_{PSS}^{u}(n)$, is generated via an inverse FFT (IFFT) operation with a subcarrier spacing of 15 kHz.

SSS, used to carry the information of the cell ID group, is constructed based on a cyclic-shift operation of maximum length sequence known as M-sequence with a length of 31.[24,26] The cyclic-shift version of even indices is scrambled by another M-sequence whose cyclic-shift index is a function of $N_{ID}^{(2)}$, and the cyclic-shift version of odd indices is scrambled by two M-sequences whose cyclic-shift indices are function of $N_{ID}^{(2)}$ and $N_{ID}^{(1)}$. SSS is transmitted earlier than PSS, that is, one OFDM symbol earlier for the FDD mode and three symbols for the TDD mode. The

frequency-mapping scheme is the same as in equation (3). PSS is repeated every 5 ms; however, the first and second SSS, transmitted, respectively, at subframes 0 and 5, are different. The difference allows detection of frame timing. SSS is generated as follows

$$\tilde{X}_{SSS}(2i) = \begin{cases} s_0^{m_0}(i)c_0(i), \text{subframe } 0 \\ s_1^{m_1}(i)c_0(i), \text{subframe } 5 \end{cases},$$

$$\tilde{X}_{SSS}(2i+1) = \begin{cases} s_1^{m_1}(i)c_1(i)z_1^{m_0}(i), \text{subframe } 0 \\ s_0^{m_0}(i)c_1(i)z_1^{m_1}(i), \text{subframe } 5 \end{cases} \qquad (4)$$

$$i = 0, 1, \ldots, 30$$

where cyclic shifts, m_0 and m_1, are given by

$$m_0 = m_3 \bmod 31, \quad m_1 = \left(m_0 + \left\lfloor \frac{m_3}{31} \right\rfloor + 1\right) \bmod 31$$

$$m_3 = N_{ID}^{(1)} + \frac{q_1(q_1+1)}{2}, \quad q_1 = \left\lfloor \frac{N_{ID}^{(1)} + q_2(q_2+1)/2}{30} \right\rfloor,$$

$$q_2 = \left\lfloor \frac{N_{ID}^{(1)}}{30} \right\rfloor$$

The basic sequence $s_r^{m_r}(i)$ and the scrambling sequence $z_1^{m_r}(i)$ are generated as follows

$$\begin{aligned} s_r^{m_r}(i) &= \tilde{s}((n + m_r) \bmod 31), \\ z_1^{m_r}(i) &= \tilde{z}((i + (m_r \bmod 8))), \quad r \in \{0, 1\} \end{aligned} \qquad (5)$$

In equation (5), the generic M-sequences, $\tilde{s}(i)$ and $\tilde{z}(i)$, are generated by linear feedback shift register (LFSR) with polynomials of $x^5 + x^2 + 1$ and $x^5 + x^4 + x^2 + x + 1$, respectively. The scrambling sequences, $c_0(i)$ and $c_1(i)$, whose generic M-sequence, $\tilde{c}(i)$, is generated by LFSR with polynomial of $x^5 + x^3 + 1$, is given by

$$c_0(n) = \tilde{c}\left(\left(n + N_{ID}^{(2)}\right) \bmod 31\right),$$

$$c_1(n) = \tilde{c}\left(\left(n + N_{ID}^{(2)} + 3\right) \bmod 31\right)$$

The MIB that consists of 24 bits is the most important broadcast information, which is transmitted on PBCH that occupies the resource grid of 72 subcarriers in the frequency domain and four OFDM symbols in the time domain.[23] MIB baseband processing is performed as follows: the 24 bits are attached with cyclic redundancy check (CRC) bits, encoded with tail biting convolutional coding, interleaved with rate matching, scrambled, mapped with quadrature phase shift keying (QPSK) modulation, precoded by a diversity precoder, mapped to the resource grid of subframe 0 for each antenna port.[24,26] For a normal CP type, the number of bits increases from 24 to 1920 after interleaving, rate matching, and 16 repetitions.
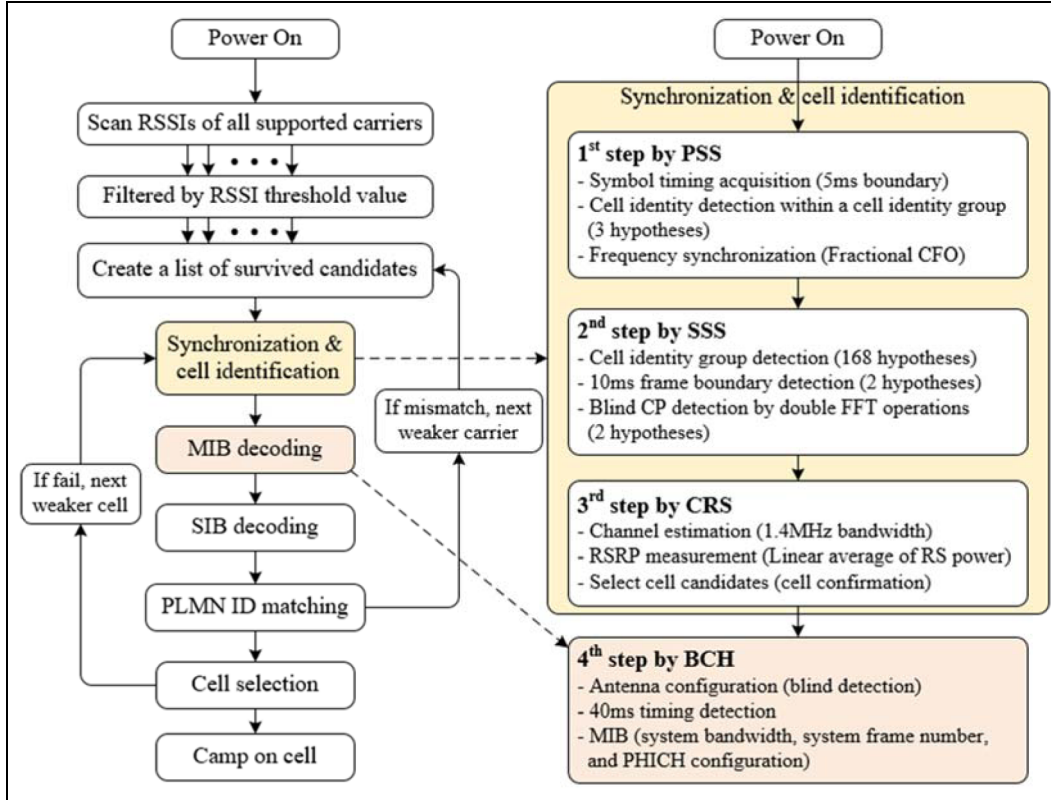
Figure 1. Complete synchronization and cell search procedure.

Note that there are 10 bits to support all 1024 frame numbers. However, only eight bits are transmitted, whereas two bits are indirectly detected at the receiver. The received signal in the time domain is given by

$$y(n) = \sum_{c=0}^{C-1} e^{j\frac{2\pi}{N}n\varepsilon_c} \sum_{l=0}^{L-1} h_l^c(n) x^c(n-l) + z(n) \qquad (6)$$

where $h_l^c(n)$, $x^c(n)$, and $z(n)$, respectively, denote the time-varying channel gain of the lth multipath component for cell c, signal transmitted from cell c, and additive white Gaussian noise (AWGN). The cell ID, N_{ID}^{Cell}, is replaced by c for notation convenience. C, L, and ε_c denote the number of neighboring cells, number of multipath components, and normalized CFO between MTC device and cell c, respectively. Here, it is assumed that the channel is static over one symbol period. The time-domain SSS and PSS modulated by the IFFT operation is given by

$$x_{sync}^c(n) = \sum_{k=-N/2}^{N/2-1} X_{sync}^c(k) e^{j\frac{2\pi}{N}nk} \qquad (7)$$

where $sync \in \{SSS, PSS\}$ denotes the subscript that indicates the synchronization signals.

Low-complexity synchronization methods for MTC devices

Because an MTC device must be compatible with legacy LTE systems, it needs to follow the cell search procedure used in the LTE system. Figure 1 shows a complete cell search procedure that will be used for the MTC device. The MTC device first needs to scan by measuring the received signal strength indicators (RSSIs) of all supported carriers for the entire bandwidth, each with 20 MHz. The measured RSSIs include the signal strength of the desired cell, interference cells, and noise. Then, RSSIs lower than the predefined threshold (or signal strength sensitivity) are filtered, resulting in a list of surviving candidates. Each surviving candidate is processed by the subsequent block until the MTC device finds a cell on which to camp. Synchronization and cell identification involve PSS and SSS detection. Using the received PSS, the MTC device acquires PSS location, cell ID within the cell ID group, and CFO. Using the received SSS, the MTC device acquires CP type, 10-ms frame boundary, and cell ID group. From MIB decoding, the MTC device acquires antenna configuration, system frame number, system bandwidth, PHICH configuration, and 40 ms frame timing. From the SIB decoding block, PLMN ID and selection criteria are decoded.

In this section, we describe the low-complexity synchronization algorithms that can reduce the power consumption of MTC devices during the synchronization period. The algorithms and decoding techniques that can be used for complete cell searching without changing the conventional ones are not discussed here. An MTC device detects the PSS location (symbol timing) by selecting the time index that corresponds to the maximum correlation output during 5 ms. By correlating the received signal with three local PSS, both the PSS location, δ, and root index, u, are jointly estimated as follows

$$(\hat{\delta}, \hat{u}) = \arg\max_{\delta, u} \left| \sum_{n=0}^{N-1} y(n + \delta) x_{\text{PSS}}^{u*}(n) \right|^2 \qquad (8)$$

where $x_{\text{PSS}}^{u*}(n)$ denotes the conjugation of time-domain local PSS selected at root index u. The M-part replica correlation method, often used in conventional LTE systems to achieve robustness against CFO, is constructed by shortening the sliding correlation window, as follows

$$(\hat{\delta}, \hat{u}) = \arg\max_{\delta, u} \frac{\sum_{m=0}^{M-1} \left| \sum_{n=mL_M}^{(m+1)L_M - 1} y(n + \delta) x_{\text{PSS}}^{u*}(n) \right|^2}{\sum_{n=0}^{N-1} |y(n + \delta)|^2}$$

$$(9)$$

where $L_M = N/M$ denotes the length of the sliding window. Note that equation (9) with M equal to one becomes equation (8) when the normalization term in the denominator of equation (9) is ignored. In general, M parallel correlators are needed for the implementation of equation (9) before combining all correlation outputs. In this article, the method for PSS detection, used in equation (9), is referred to as "Method P1." When $M = 2$, Method P1 can be expresses as follows

$$\frac{R_0(\delta) + R_1(\delta)}{P(\delta)}$$
$$= \frac{\left| \sum_{n=0}^{L_M-1} y(n + \delta) x_{\text{PSS}}^{u*}(n) \right|^2 + \left| \sum_{n=0}^{L_M-1} y(n + L_M + \delta) x_{\text{PSS}}^{u*}(n + L_M) \right|^2}{\sum_{n=0}^{N-1} |y(n + \delta)|^2}$$

$$(10)$$

Note that two linear-shift cross correlators, $R_0(\delta)$ and $R_1(\delta)$, start at a different time index and there exists L_M samples offset between the two correlators. In addition, the sliding window is reduced to L_M samples, and each local PSS is divided into two parts. In the first correlator $R_0(\delta)$, the first part of PSS that corresponds to the first L_M samples is correlated with the received signal that starts at the nth instant. In the second correlator $R_1(\delta)$, the second part of PSS that corresponds to the second L_M samples is correlated with the received signal that starts at the $(n + L_M)$th instant. Figure 2 shows the proposed method for PSS detection, referred
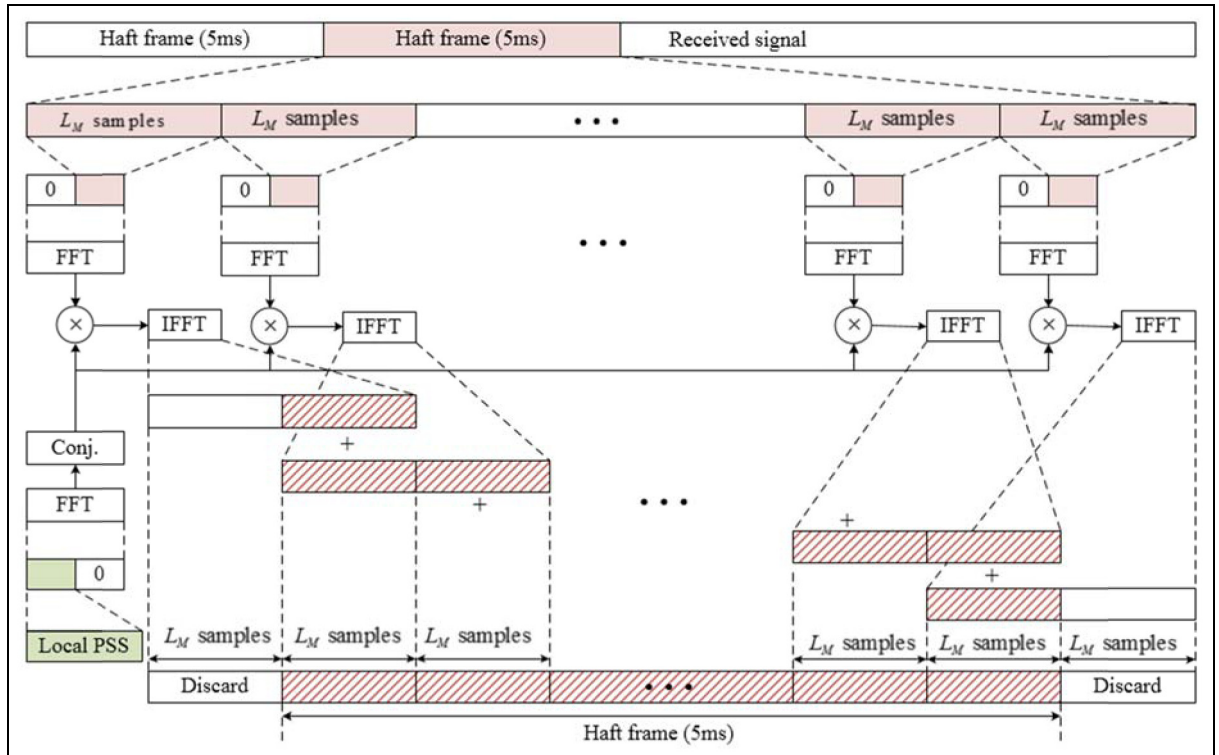

Figure 2. Method P2 for PSS detection.

Table 1. Computational complexity for PSS detection.

Method	Number of complex multiplications	Examples	
		$M = 1$	$M = 2$
Method P1	$3MN_SN$	3,686,400	7,372,800
Method P2	$3M(3N_S\log_2 2L_M + 2L_M)$	604,928	1,209,856

PSS: primary synchronization signal.

MIB content	Number of bits	Frequency of change
System bandwidth	3	Infrequently
PHICH configuration	3	Infrequently
System frame number	8	Change every 40 ms
Reserve bits	10	Set to 0 by RRC

to as "Method P2" in this article. In Figure 2, only the operation with the first part of PSS in the period of 5 ms is shown. As shown in Figure 2, the received signal is first divided into small blocks with L_M samples each. Then, each block is padded with L_M zero values at the front. The extended block is transformed into the frequency domain via FFT operation of size $2L_M$. In addition, the local PSS is padded with L_M zero values at the last, followed by a FFT and conjugation operation. The two signals are multiplied in the frequency domain, followed by transformation via IFFT operation. The time-domain signal of each block is added in an overlapped manner. Finally, L_M samples on both sides are discarded. Table 1 lists the number of complex multiplications required for PSS detection.

Here, N_S denotes the number of samples within the window. In this example, the value of N_S is set to 9600 acquired at the sampling rate of 1.92 MHz during the 5 ms period. Computational complexities are compared for two different cases of M. The complexity required for calculating the normalization term in the denominator is not included for both methods. From this table, one can see that there are six times fewer complex multiplications for Method P2 than for Method P1 when $N = 128$.

Figure 3 shows the SSS detection procedure. Here, the received time-domain SSS for each block is slid at a different window size and timing offset, depending on the type of hypothesis (normal and extended CP hypotheses). After finishing CP-type detection, CP is used for CFO estimation. The accuracy of CFO estimation can be improved by measuring the signal over a period of more than two OFDM symbols (CPs of both PSS and SSS) at the correct timing and CP length. If the CFO value is accurately estimated by the received PSS, the CP-based CFO estimation block is unnecessary. Then, SSS is compensated by the estimated value
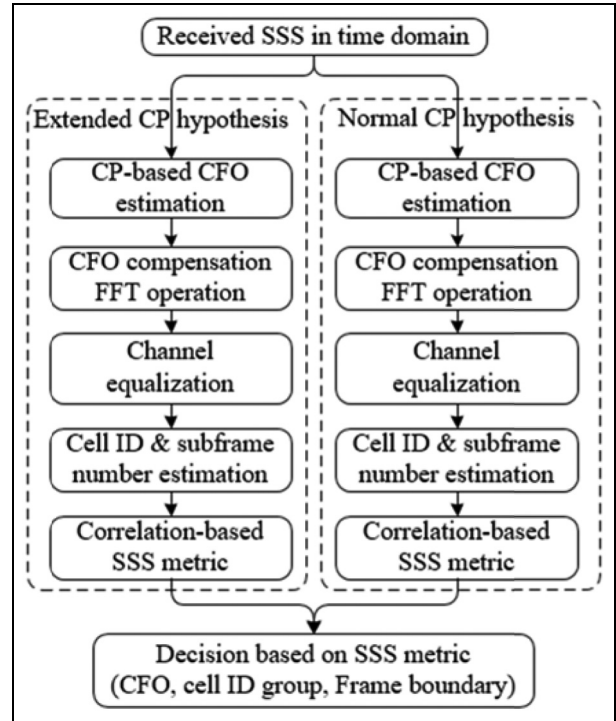
Figure 3. SSS detection procedure.

of CFO before it is transformed to the frequency domain. For a coherent detection case, the channel equalization block is mandatory. The block is not required for non-coherent detection cases. Next, the cell ID group number and subframe index (either 0 or 5) that carry SSS are estimated by correlating the received SSS with 168 local SSS in the frequency domain. This block requires the highest computational complexity, because SSS metrics need to be calculated by correlating the received SSS with all possible candidates. If the duplexing mode, either FFD or TDD, is not known to the MTC device, duplexing mode detection is required using the SSS metrics.

Here, we focus on the estimation method for the cell ID group and subframe index in order to reduce the computational complexity required to obtain the SSS metrics. Figure 4 shows the overall detection procedure for the cell ID group and subframe index. In Figure 4, the received SSS with 62 subcarriers is divided into two sequences, each with 31-length sequence on even
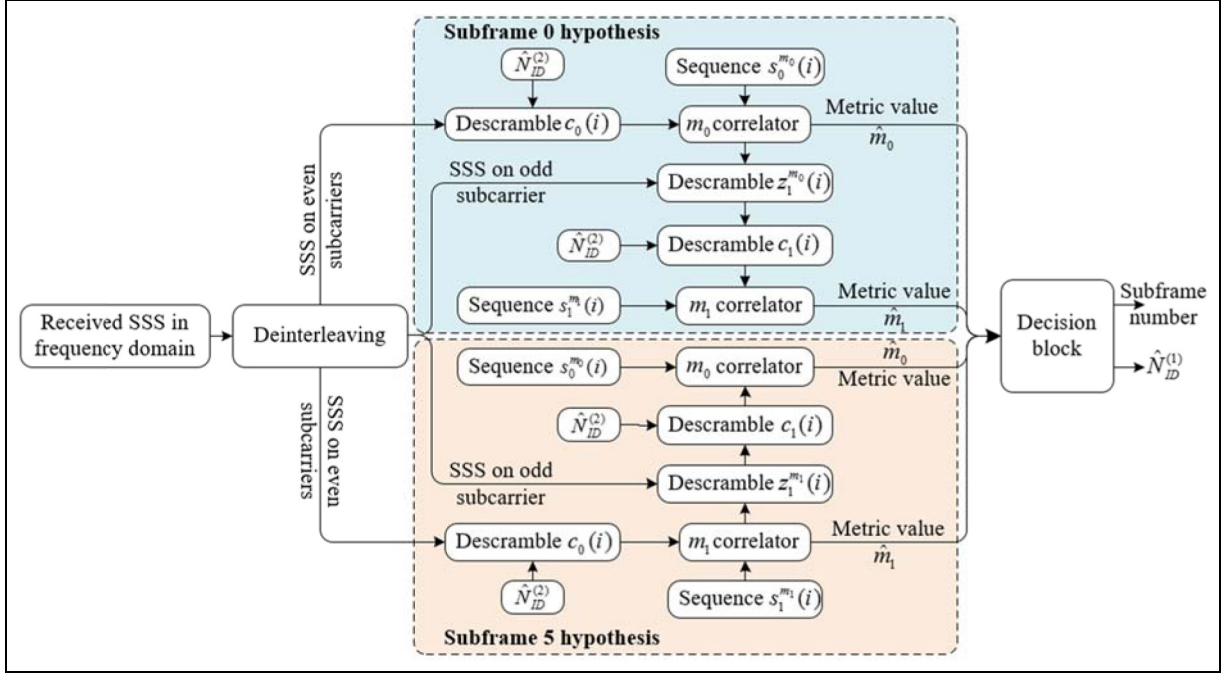
Figure 4. Detection procedure for cell ID group and subframe number.

and odd subcarrier indices. After descrambling, each sequence is processed by different correlators to estimate indices m_0 and m_1 for detection of the cell ID group. As seen in the figure, there are two hypotheses that correspond to the two subframe indices (subframes 0 and 5). The indices m_0 and m_1 are estimated in each block before making a decision based on the metric values.

For hypothesis subframe 0, m_0 is first estimated, and then m_1 is estimated using $z_1^{m_0}(i)$ and $c_1(i)$-descrambled SSS. For hypothesis subframe 5, the process is reversed by estimating m_1 first and then m_0. For hypothesis subframe 0, m_0 and m_1 are estimated by the following equation

$$\hat{m}_0 = \underset{m_0 \in \{0, 1, ..., 29\}}{\arg\max} \left| \sum_{i=0}^{30} Y_{\text{SSS}}^{\text{even}}(i) s_0^{m_0}(i) \right|^2,$$

$$\hat{m}_1 = \underset{m_1 \in \{0, 1, ..., 30\}}{\arg\max} \left| \sum_{i=0}^{30} Y_{\text{SSS}}^{\text{odd}}(i) s_1^{m_1}(i) \right|^2 \tag{11}$$

where $Y_{\text{SSS}}^{\text{even}}(i)$ and $Y_{\text{SSS}}^{\text{odd}}(i)$ denote the received SSS after descrambling on even and odd subcarriers, respectively. For subframe 0, $Y_{\text{SSS}}^{\text{even}}(i)$ is descrambled by $c_0(i)$, and $Y_{\text{SSS}}^{\text{odd}}(i)$ is descrambled by $z_1^{m_0}(i)$ and $c_1(i)$. For hypothesis subframe 5, m_0 and m_1 are estimated in a reverse manner by the following equation

$$\hat{m}_1 = \underset{m_1 \in \{0, 1, ..., 30\}}{\arg\max} \left| \sum_{i=0}^{30} Y_{\text{SSS}}^{\text{even}}(i) s_1^{m_1}(i) \right|^2,$$

$$\hat{m}_0 = \underset{m_0 \in \{0, 1, ..., 29\}}{\arg\max} \left| \sum_{i=0}^{30} Y_{\text{SSS}}^{\text{odd}}(i) s_0^{m_0}(i) \right|^2 \tag{12}$$

By comparing the SSS metrics obtained from the two subframe blocks, the synchronization parameters associated with SSS are finally determined. Note that 10-ms frame boundary can be indirectly obtained from the estimated subframe numbers. In this article, the conventional method for obtaining SSS metrics at the M-sequence level, equations (11) and (12), is referred to as "Method S1."

Next, a method for SSS detection using the fast Hadamard transform (FHT) operation, referred to as "Method S2" in this article, is proposed. The FHT operation is used to reduce the computational complexity required to obtain SSS metrics. In order to use the FHT operation, the indices of each sequence need to be modified by a permutation operation. The permutation operation is not regarded as a multiplication operation, because it changes only the sequence indices. However, the permutation operation is expressed by matrix multiplication with a permutation matrix for notation convenience. The FHT operation that involves only an additive operation can be used to estimate indices m_0 and m_1, for detection of the cell ID group, as indicated in Table 2. Permutation matrices $\mathbf{P}_S$ and $\mathbf{P}_L$ in Table 2 are generated from the M-sequence of length 32.[27,28] Here, $\mathbf{Y}_{\text{SSS}}^{\text{even/odd}} = [0, Y_{\text{SSS}}^{\text{even/odd}}(0), \ldots, Y_{\text{SSS}}^{\text{even/odd}}(30)]^T$ denote a received signal vector by padding one zero-value at the first element. The superscript even/odd in the received signal vector represents the case of a received SSS with even/odd index, respectively. For subframe 0, the indices m_0 and m_1 are estimated by

Table 2. Low-complexity cell ID group estimator.

Generate 32×32 permutation matrix, $\mathbf{P}_S$, $\mathbf{P}_L$

Reorder received SSS vector using $\mathbf{P}_S$

$\tilde{\mathbf{Y}}_{SSS}^{even/odd} \leftarrow \mathbf{P}_S \mathbf{Y}_{SSS}^{even/odd}$

Initializing 30×1 correlation vector, $\mathbf{R}^{even/odd}$

Initializing 16×1 vector, $\mathbf{Y}_{add}^{even/odd}$, $\mathbf{Y}_{substract}^{even/odd}$

For iteration = 1:5

     $\tilde{\mathbf{Y}}_{add}^{even/odd} \leftarrow \left[\tilde{\mathbf{Y}}_{SSS}^{even/odd}\right]_{1:16} + \left[\tilde{\mathbf{Y}}_{SSS}^{even/odd}\right]_{17:32}$

     $\tilde{\mathbf{Y}}_{substract}^{even/odd} \leftarrow \left[\tilde{\mathbf{Y}}_{SSS}^{even/odd}\right]_{1:16} - \left[\tilde{\mathbf{Y}}_{SSS}^{even/odd}\right]_{17:32}$

     Update received SSS vector

     Even index: $\left[\tilde{\mathbf{Y}}_{SSS}^{even/odd}\right]_{1:2:32} \leftarrow \tilde{\mathbf{Y}}_{add}^{even/odd}$

     Odd index: $\left[\tilde{\mathbf{Y}}_{SSS}^{even/odd}\right]_{2:2:32} \leftarrow \tilde{\mathbf{Y}}_{substract}^{even/odd}$

End

If index is even

     $\mathbf{R}^{even} \leftarrow \left[\mathbf{P}_L \tilde{\mathbf{Y}}_{SSS}^{even}\right]_{2:31}$

Else

     $\mathbf{R}^{odd} \leftarrow \left[\mathbf{P}_L \tilde{\mathbf{Y}}_{SSS}^{odd}\right]_{3:32}$

End

SSS: secondary synchronization signal.

$$\hat{m}_0 = \underset{m_0 \in \{1,2,...,30\}}{\arg\max} \left|\mathbf{R}^{even}\right|_{m_0}^2, \quad \hat{m}_1 = \underset{m_1 \in \{1,2,...,30\}}{\arg\max} \left|\mathbf{R}^{odd}\right|_{m_1}^2 \tag{13}$$

As shown in equation (13), the index that maximizes the correlation vector, $\mathbf{R}^{even/odd}$, is selected. After index selection, the estimates for indices m_0 and m_1 are replaced by $\hat{m}_0 - 1$ and $\hat{m}_1$, respectively. The index selection for subframe 5 can be processed similarly.

Table 3 indicates the computational complexity required for SSS detection. In Table 3, N_{SB} and N_{sym} denote the number of scrambling blocks (SBs) in Figure 4 and the number of CPs used for CFO estimation, respectively. The values of N_{SB} and N_{sym} are set to 3 and 2, respectively. Here, one scrambling operation is counted as one multiplication operation. The

computational complexity for N-point FFT is given by $(N/2)\log_2 N$. From this table, one can see that the computational complexity required for SSS detection is significantly reduced by the proposed method (Method S2). There are five times fewer multiplications and 2.8 fewer additions for Method S2 than for Method S1.

After estimating the cell ID group, reference signal received powers (RSRPs) that correspond to candidate cell IDs are measured from reference signals. RSRP reflects the signal strength of each cell, which provides the selection of the serving cell. RSRP, obtained by a linear average of reference signal power in the available resource grid, is defined for cell c as follows

$$\text{RSRP}(c) = \sum_{s=0}^{N_T-1} \sum_{r=0}^{N_F-1} \left|Y_{l_s}\left(k_r^c\right)\right|^2 \tag{14}$$

where $Y_{l_s}(k_r^c)$ denotes the received reference signal measured at subcarrier index k_r^c of the l_sth OFDM symbol for cell ID c. N_T and N_F denote the number of OFDM symbols and number of subcarriers carrying the reference signal, respectively. For an MTC device with minimum bandwidth, $N_T = 4$, $N_F = 12$, and $l_s \in \{0, 4, 7, 12\}$ in the case of a normal CP. A cell-specific shift is given by $c \bmod 6 = 0$. The resource element allocation for reference signals cycles once every six physical cell ID values, that is, cell ID values that are integer multiples of six have the same resource element allocation as cell ID 0. A differential correlation technique can be used to randomize the interferences and cancel the phase distortion caused by either channel or symbol timing offset as follows

$$\text{RSRP}(c) = |\text{rsrp}(c)| \tag{15}$$

where

$$\text{rsrp}(c) = \frac{\sum_{s=0}^{N_T-1}\sum_{r=0}^{N_F-1} Y_{l_s}^*(k_r^c)Y_{l_s}(k_{r+1}^c)P_c(r,s)P_c^*(r+1,s)}{\sum_{s=0}^{N_T-1}\sum_{r=0}^{N_F-1}\left|Y_{l_s}(k_r^c)\right|^2}$$

Table 3. Computational complexity for SSS detection.

Method	Number of complex multiplications	Number of complex additions	Numerical example	
			Multiplications	Additions
Correlation	$C_1 = 2(62N_{SB} + 3600)$	7200	7572	7200
FHT operation	$C_2 = 124N_{SB}$	$256\log_2 32 = 1280$	384	1280
CFO estimation	$C_3 = 9N_{sym} + 32N_{sym}$	$A_1 = 9N_{sym} + 32N_{sym}$	82	82
CFO compensation and FFT operation	$C_4 = 2N + N\log_2 N$	$A_2 = 2N\log_2 N$	1152	1792
SSS metric	122	122	122	122
Total in Method S1	$C_1 + C_3 + C_4 + 122$	$A_1 + A_2 + 7200 + 122$	8928	9196
Total in Method S2	$C_2 + C_3 + C_4 + 122$	$A_1 + A_2 + 1280 + 122$	1740	3276

SSS: secondary synchronization signal; FFT: fast Fourier transform; CFO: carrier frequency offset; FHT: fast Hadamard transform.
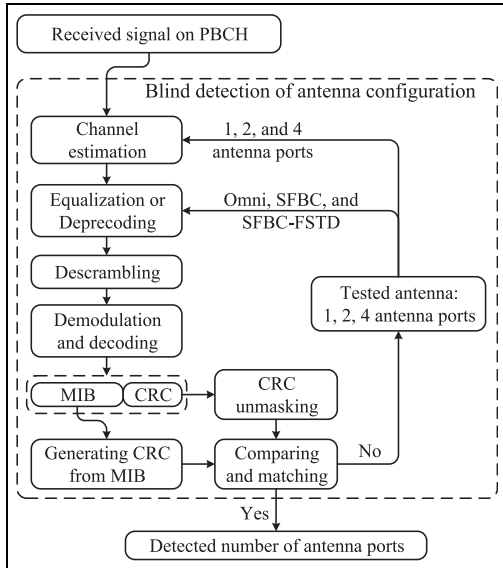
Figure 5. Antenna configuration detection procedure using CRC.

Here, $P_c(r, s)$ denotes the reference signal at the pair indices (r, s) selected for cell ID c.

After selecting the candidate cell based on the RSRP measurement, the MTC device decodes MIB for the system bandwidth, PHICH configuration, and system frame number. In addition, the MTC device needs to acquire more information on the cell, such as antenna configuration and 40-ms frame boundary. Note that the MTC device cannot obtain receive diversity gain (only one receive antenna), but it can still obtain transmit diversity gain (many transmit antennas at eNodeB). Figure 5 shows the procedure of antenna configuration detection using CRC. As shown in Figure 5, eNodeB uses a two-antenna-port configuration for space-frequency block coding (SFBC) transmit diversity and a four-antenna-port configuration for combination of space-frequency block coding and frequency-switch transmit diversity (SFBC-FSTD). Therefore, there exist three hypotheses on antenna-port configurations: one, two, and four antenna ports. In order to detect the antenna configuration, the MTC device starts with one antenna-port configuration by estimating the channel using the reference signals at the minimum bandwidth. Subsequently, equalization, descrambling, demodulation and decoding, and CRC unmasking are performed. The local and unmasked CRCs are then compared for antenna configuration detection. Next, the MTC device detects 40-ms frame boundary by softly combining signals with 16 repetitive patterns and decoding MIB three times while shifting the window. With this scheme, we can obtain a combining gain with a processing delay of 70 ms. The 40-ms frame boundary can be also detected by descrambling the received MIB with four possible

descrambling sequences.[24] In this scheme, we cannot obtain the combining gain. However, the processing delay for decoding MIB can be reduced to 10 ms.

The DRX mechanism in the LTE system allows a terminal device to conserve battery power and increase overall system capacity. A DRX cycle consists of an "On Duration," during which the terminal device monitors the downlink channel, and a "DRX period," during which a terminal device can omit reception of downlink channels for battery-saving purposes.[19] The terminal device achieves power saving by switching off most of its circuitries during the DRX period. DRX parameters, such as DRX inactivity timer, short DRX cycle, DRX short cycle timer, long DRX cycle, On Duration timer, DRX offset, and retransmission timer, are controlled by the networks.[20] In order to support the ultra-low-power consumption required by the MTC device, the duration of the DRX period is extended up to several minutes, implying that it can go to deep sleep mode while turning off most of its radio chip to conserve battery life.[29] When the MTC device loses its synchronization during the DRX period, it does not need to go back to the initial point, because it can start synchronization and cell search with the carrier selected previously. Unlike mobile UE, the MTC device in a DRX cycle, usually installed in a fixed location, does not need the process of neighboring cell search. Therefore, the MTC device in a DRX cycle can save additional battery power by omitting these steps and applying the low-complexity synchronization methods developed in this article when it wakes up.

Simulation

In this section, we evaluate the performance of the proposed synchronization methods for MTC devices in the LTE environment using MATLAB.[26,30] All simulation parameters are taken from the LTE specification.[23,24,31] It is assumed that the MTC device supports low-data rate and low-mobility operation.[14,29] The following parameters are used for the simulation: bandwidth of 1.4 MHz, sampling rate of 1.92 MHz, and FFT size of 128. The FDD frame structure with normal CP type is used. It is assumed that both MTC device and eNodeB employ one antenna, implying that no transmit diversity gain is obtained. Because MTC devices are usually installed in a fixed position, the performance is evaluated under near static multipath fading channel (Extended Pedestrian A (EPA): 0/5 Hz and Extended Vehicular A (EVA): 0/5 Hz). In this section, performance results are shown only for the proposed synchronization methods (PSS and SSS detections). Other results (symbol timing, CFO, CP type, framing timing, and antenna configuration detection) that can be obtained by the conventional synchronization and cell
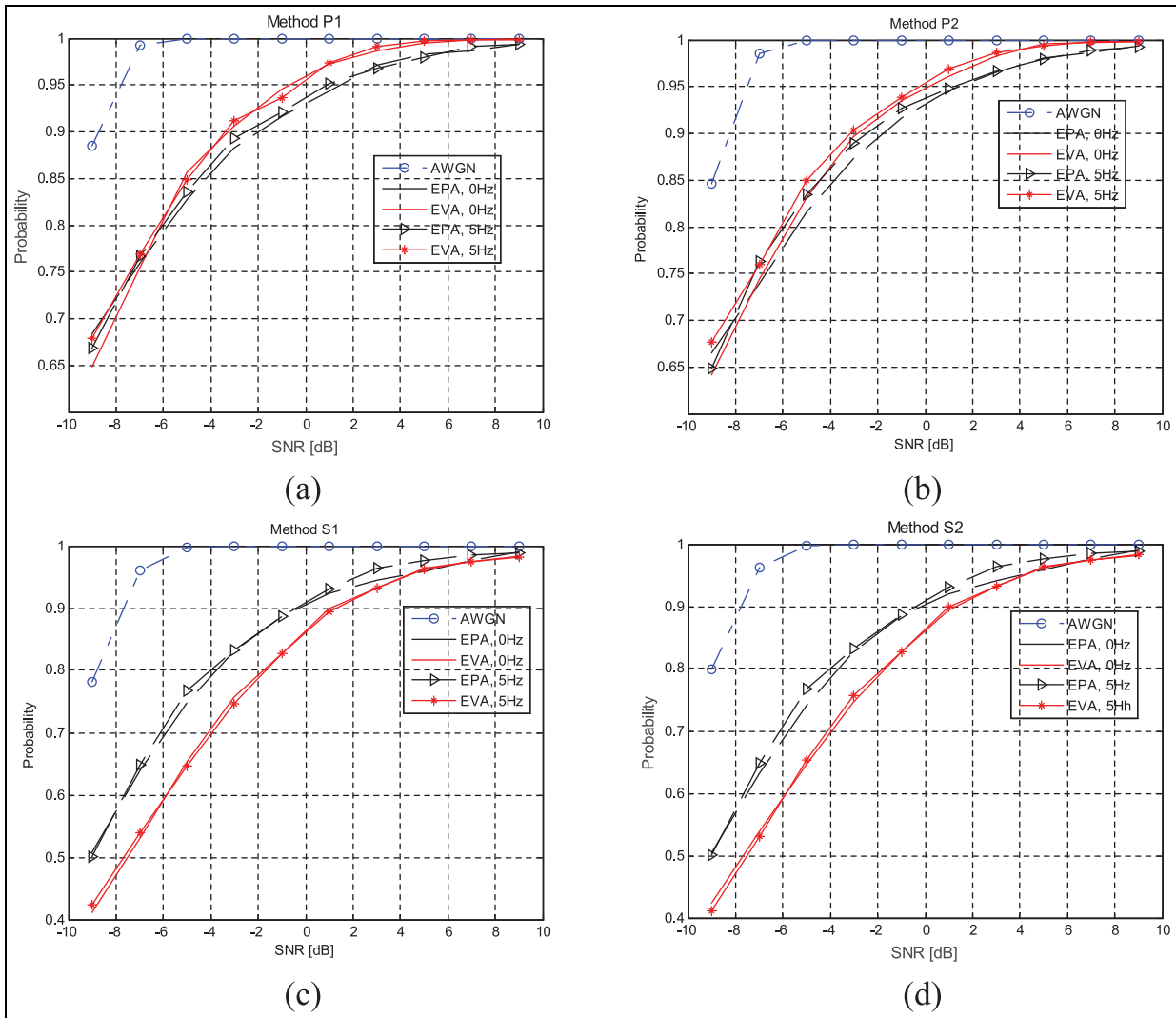
Figure 6. Detection probabilities of PSS and SSS: (a) PSS detection with Method P1, (b) PSS detection with Method P2, (c) SSS detection with Method S1, and (d) SSS detection with Method S1.

search method used in the LTE system are not discussed.

Figure 6 shows the probabilities of PSS and SSS detection in the AWGN, EPA, and EVA channel environments. In Figure 6(a) and (b), the probability of PSS detection is shown with M equal to one. In these figures, 0 Hz (5 Hz) implies that the channel is a static (near static) multipath fading channel. Performances are evaluated over 1000 realizations of AWGN and multipath fading channels. In each realization, the channel power delay profile (PDP) is changed with different amplitude values of the multipath component, each experiencing Rayleigh fading. From Figure 6(a) and (b), one can see that the performances of Methods P1 and P2 are similar in all channels. The PSS detection probabilities of both methods in the AWGN channel reach 1 at a signal-to-noise ratio (SNR) of -5 dB, whereas those in the multipath fading channels reach 1

at an SNR of 10 dB. For example, 950 (0.95×1000) MTC devices out of 1000 can correctly detect the root index of PSS at the SNR of 2 dB. Figure 6(c) and (d) show the probability of SSS detection when the parameters associated with PSS (cell ID within cell ID group and PSS location) are estimated correctly.

From these figures, one can see that the performances of Methods S1 and S2 are similar in all channels. The performances of both methods are degraded slightly in all channels because both methods are based on coherent detection, and the channel estimates obtained from PSS are not accurate. In multipath fading channels, 910 (0.91×1000) MTC devices can detect the cell ID group correctly at an SNR of 2 dB.

Figure 7 shows bit error rate (BER) and block error rate (BLER) for MIB decoding in the AWGN channel. BLER is defined as the ratio of the number of block errors to the number of total realizations (1000). Block
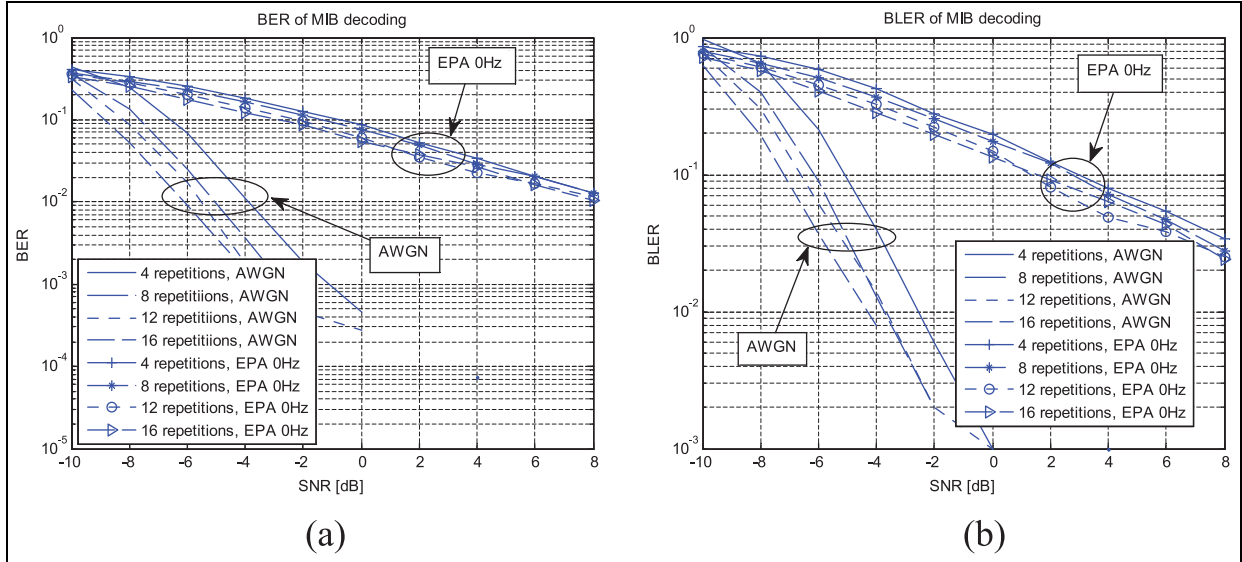
Figure 7. Performances for MIB decoding: (a) BER and (b) BLER.

error detection is based on the CRC error detection mechanism. The number of bits used in BER calculation is the number of bits per block multiplied by the realization number (40×1000). For MIB decoding, the Viterbi decoding algorithm with soft-combining log-likelihood ratio (LLR) is used. As can be seen from the figure, performance improves as the number of repetitions increases. No error occurs when SNR is higher than 0 dB.

Figure 8 shows the computational complexities required for PSS and SSS detection when the number of subcarriers varies. Figure 8(a) shows the number of complex multiplications required for PSS detection in the 5-ms period. From this figure, one can see that there are fewer complex multiplications for Method P2 than for Method P1, and the gap increases as the number of subcarriers increases. Figure 8(b) and (c) shows the number of complex multiplications and additions required for SSS detection, respectively. From these figures, one can also see that there are fewer complex multiplications for Method S2 than for Method S1. From these figures, one can see that Method P2 and Method S2 are appropriate for the synchronization of low-power MTC devices.

The power consumption varies depending on the design architecture of the digital circuit cell, including adders, multipliers, and accumulators.[32–35] To compare the performance in terms of power consumption, a multiplier based on the latch adder (LA), proposed in Chong et al.,[35] is used in this article. The multiplier based on the LA was developed specifically for low-voltage power-critical low-speed applications in which the clock speed is lower than 5 MHz. Here, it is assumed that the signal amplitude is quantized at the 16-bit level, resulting in 16-bit arithmetic operation. All

of the designs are based on the 0.35-μm complementary metal-oxide semiconductor (CMOS) fabrication process. For low-voltage (1.1 V) and low-speed ($<$5 MHz) applications, the power dissipation of one multiplication in Chong et al.[35] is 18.8 μW/MHz for a 16 $\times$ 16-bit multiplier. Additionally, the power dissipation of one LA is 10.1 $\times$ 10^{-8} W/MHz for one-bit operation. Therefore, the power dissipation for 16-bit operation is 1.616 μW/MHz (16 $\times$ 10.1 $\times$ 10^{-8} W/MHz). Figure 9 shows the power consumption required for PSS and SSS detections for different numbers of carriers. Here, the unit of power consumption is dBW/MHz (decibel Watt per MHz). The parameters in Tables 1 and 3 are used for calculation of the power consumption required for PSS and SSS detections, respectively. It is also assumed that one complex multiplication requires four real multiplications along with two real additions. Figure 9(a) shows the power consumption required for PSS detection when Methods P1 and P2 are used. It can be seen from this figure that the proposed method for PSS detection requires 8 dB less power consumption than the conventional method, regardless of the number of carriers and the value of M. Figure 9(b) shows the power consumption required for SSS detection when Methods S1 and S2 are used. This figure shows that the proposed method for SSS detection requires 7 dB less power consumption than the conventional method, regardless of the number of carriers.

Conclusion

In this article, a complete synchronization and cell search procedure was described for MTC devices in LTE systems. Low-complexity algorithms for PSS and SSS detection were also proposed for low-power MTC
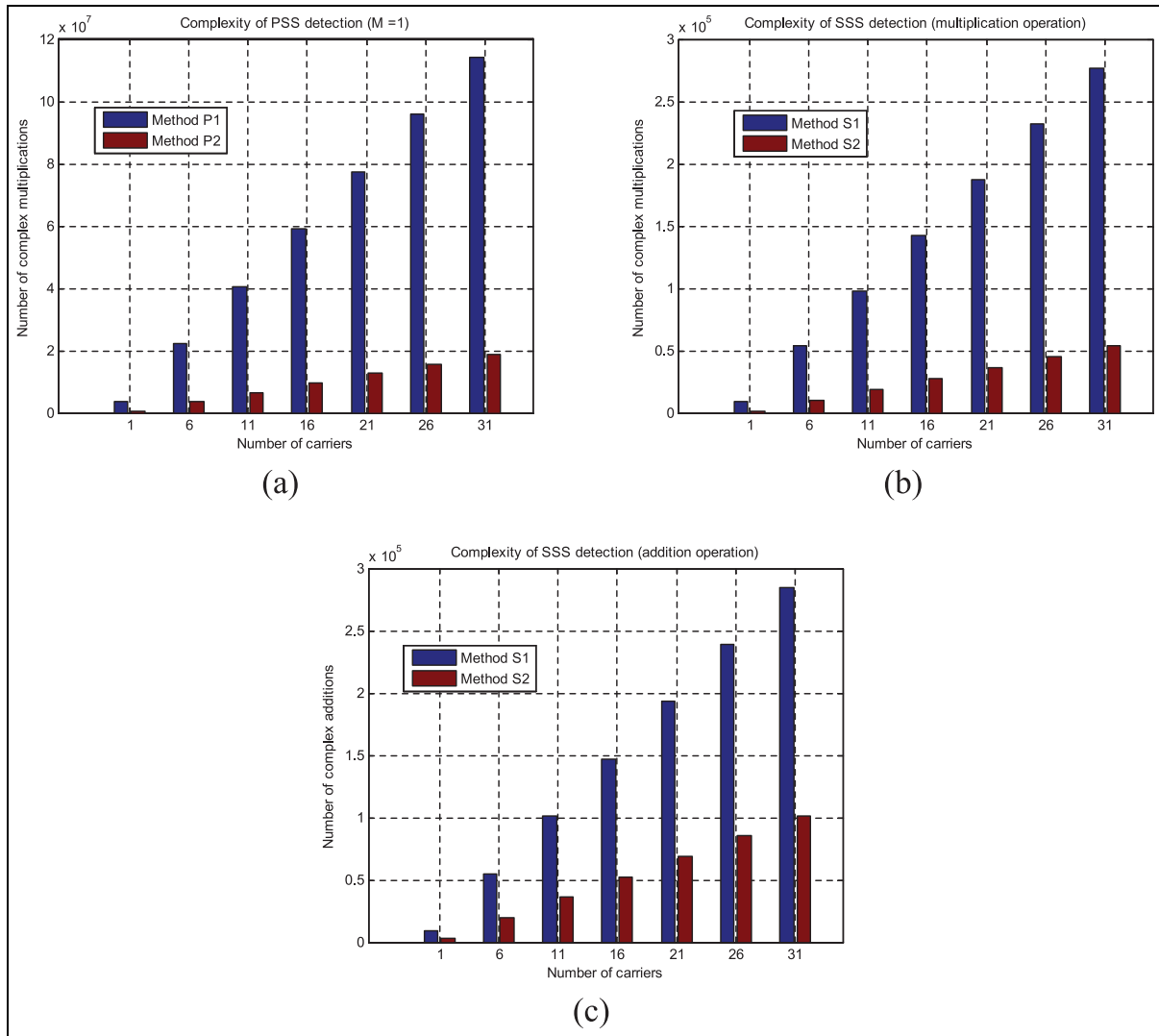
Figure 8. Computational complexity for PSS and SSS detections: (a) multiplication operation for PSS detection, (b) multiplication operation for SSS detection, and (c) addition operation for SSS detection.
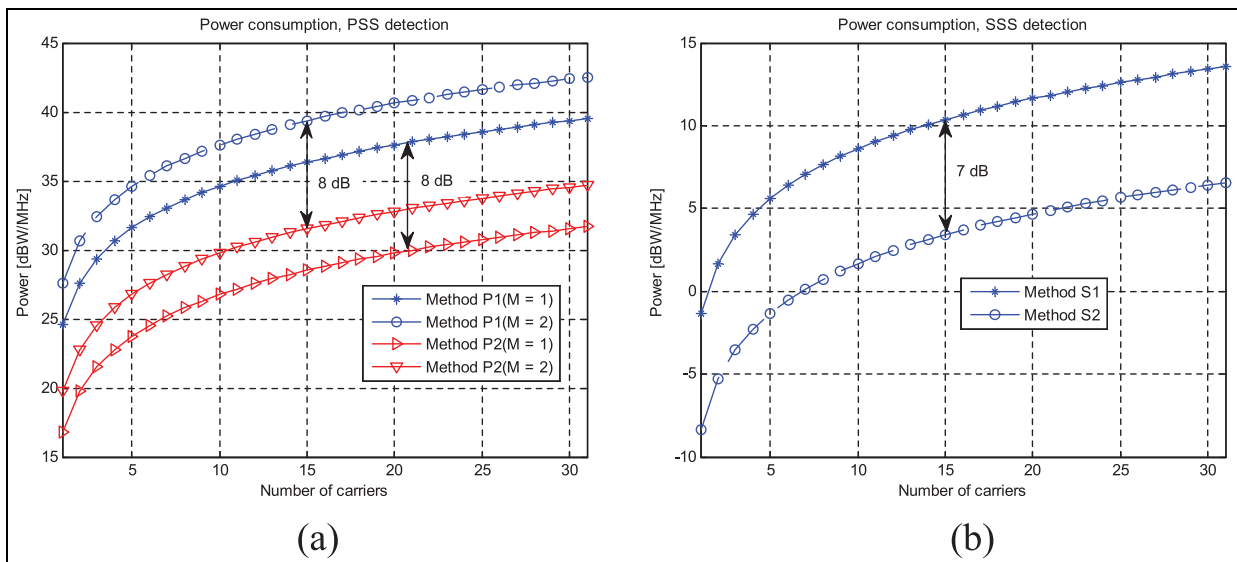

Figure 9. Power consumption required for (a) PSS and (b) SSS detections.

devices. It was shown by simulation under LTE-based MTC environments that the proposed method for PSS detection (Method P2) requires six times fewer complex multiplications than the conventional method (Method P1), whereas the performances of Methods P1 and P2 are similar. It was also shown that the proposed method for SSS detection (Method S2) requires five times fewer multiplications than the conventional method (Method S1), whereas the performances of Methods S1 and S2 are similar. The proposed algorithms allow MTC devices in a DRX cycle to resynchronize quickly with less power when synchronization is lost during a deep sleep period.

Declaration of conflicting interests

Funding

References

1. Xu LD, He W and Li S. Internet of things in industries: a survey. *IEEE T Ind Inform* 2014; 10(4): 2233–2243.
2. Palattella MR, Dohler M, Grieco A, et al. Internet of things in the 5G era: enablers, architecture, and business models. *IEEE J Sel Area Comm* 2016; 34(3): 510–526.
3. Zanella A, Bui N, Castellani A, et al. Internet of things for smart cities. *IEEE Internet Thing J* 2014; 1(1): 22–32.
4. Shariatmadari H, Ratasuk R, Iraji S, et al. Machine-type communications: current status and future perspectives toward 5G systems. *IEEE Commun Mag* 2015; 53(9): 10–17.
5. Ratasuk R, Magalvedhe N and Ghosh A. Overview of LTE enhancements for cellular IoT. In: *Proceedings of the 2015 IEEE 26th annual international symposium on personal, indoor, and mobile radio communications (PIMRC)*, Hong Kong, 30 August–2 September 2015. New York: IEEE.
6. Haro CA and Dohler M. *Machine-to-machine (M2M) communications: architecture, performance and applications*. Amsterdam: Elsevier, 2015.
7. Lo A, Law YW and Jacobsson M. A cellular-centric service architecture for machine-to-machine (M2M) communications. *IEEE Wirel Commun* 2013; 20(5): 143–151.
8. Lien SY, Chen KC and Lin Y. Toward ubiquitous massive accesses in 3GPP machine-to-machine communications. *IEEE Commun Mag* 2011; 49(4): 66–74.
9. Taleb T and Kunz A. Machine type communications in 3GPP networks: potential, challenges, and solutions. *IEEE Commun Mag* 2012; 50(3): 178–184.
10. Jain P, Hedman P and Zisimopoulos H. Machine type communications in 3GPP systems. *IEEE Commun Mag* 2012; 50(11): 28–35.
11. Astely D, Dahman E, Fodor G, et al. LTE release 12 and beyond. *IEEE Commun Mag* 2013; 51(7): 154–160.
12. Lassila POP, Aalto S, Larmo A, et al. Analysis of PDCCH performance for M2M traffic in LTE. *IEEE T Veh Technol* 2014; 63(9): 4357–4437.
13. 3GPP v0.2.3. *Standardization of machine-type communications* (Technical report). Sophia Antipolis: 3GPP, 2014.
14. Ali A, Hamouda W and Uysal M. Next generation M2M cellular networks: challenges and practical considerations. *IEEE Commun Mag* 2015; 53(9): 18–24.
15. Chang K, Soong A, Tseng M, et al. Global wireless machine-to-machine standardization. *IEEE Internet Comput* 2011; 15(2): 64–69.
16. Misic VB and Misic J. *Machine-to-machine communications: architecture, technology, standards, and application*. Boca Raton, FL: CRC Press, 2015.
17. Wang K, Jesus JAZ and Dohler M. Energy-efficiency of LTE for small data machine-to-machine communications. In: *Proceedings of the 2013 IEEE International Conference on Communications (ICC)*, Budapest, 9–13 June 2013. New York: IEEE.
18. Popp J, Robert J and Heuberger A. Energy consumption of low data rate M2M communications in LTE. In: *Proceedings of the European conference on smart objects, systems and technologies smart SysTech 2015*, Aachen, 16–17 July 2015. New York: IEEE.
19. Bontu CS and Nortel EI. DRX mechanism for power saving in LTE. *IEEE Commun Mag* 2009; 47(6): 48–55.
20. Zhou K, Nikaein N and Spyropoulos T. LTE/LTE-A discontinuous reception modeling for machine type communications. *IEEE Wirel Commun Lett* 2013; 2(1): 102–105.
21. Balasubramanya NM, Lampe L and Bennett S. DRX with quick sleeping: a novel mechanism for energy-efficient IoT using LTE/LTE-A. *IEEE Internet Thing J* 2016; 3: 398–407.
22. Cho YS, Kim J, Yang WY, et al. *MIMO-OFDM wireless communications with MATLAB*. Chichester: Wiley, 2010.
23. Dahlman E, Parkvall S and Skold J. *4G: LTE/LTE-advanced for mobile broadband*. Amsterdam: Elsevier, 2011.
24. Sesia S, Toufik I and Baker M. *LTE—the UTMS long term evolution: from theory to practice*. Chichester: Wiley, 2011.
25. Ahmadi S. *LTE-advanced: a practical systems approach to understanding the 3GPP LTE releases 10 and 11 radio access technologies*. Amsterdam: Elsevier, 2014.
26. 3GPP TS 36.211. *Physical channels and modulation* (Technical report). Sophia Antipolis: 3GPP, 2016.
27. Cohn M and Lempel A. On fast M-sequence transforms. *IEEE T Inform Theory* 1977; 23: 135–137.
28. Anshi C, Di L and Renzhong Z. A research on fast Hadamard transform (FHT) digital systems. In: *Proceedings of the 1993 IEEE region 10 conference on computer, communication, control and power engineering*

(TENCON), 1993, Beijing, China, 19–21 October 1993, vol. 3, pp.541–545. New York: IEEE.

29. Qualcomm. LTE MTC: optimizing LTE advanced for machine-type communications, November 2014, https://www.qualcomm.com/documents/lte-mtc-optimizing-lte-advanced-machine-type-communications

30. Zarrinkoub H. *Understanding LTE with MATLAB: from mathematical modeling to simulation and prototyping*. Chichester: Wiley, 2014.

31. 3GPP TS 36.104. *Base station radio transmission and reception* (Technical specification). Sophia Antipolis: 3GPP, 2012.

32. Zhang X, Boussaid F and Bermak A. 32 bit × 32 bit multiprecision razor-based dynamic voltage scaling multiplier with operands scheduler. *IEEE T VLSI Syst* 2014; 22(4): 759–770.

33. Hsu SK, Mathew SK, Anders MA, et al. A 110 GOPS/W 16-bit multiplier and reconfigurable PLA loop in 90-nm CMOS. *IEEE J Solid-St Circ* 2006; 41(1): 256–264.

34. Petra N, Caro DD, Garofalo V, et al. A truncated binary multipliers with variable correction and minimum mean square error. *IEEE T Circuits: I* 2010; 57(6): 1312–1325.

35. Chong KS, Gwee BH and Chang JS. A micropower low-voltage multiplier with reduced spurious switching. *IEEE T VLSI Syst* 2005; 13(2): 255–265.